

## AX\_LOAD: A COMPUTER CODE TO MODEL CONSTRAINED FUEL STRING AXIAL EXPANSION

J.K. CHAN, H.E. SILLS, and V.J. LANGMAN

Reactor Safety and Operational Analysis Department, Ontario Hydro  
700 University Ave., Toronto, Ontario, M5G 1X6

### ABSTRACT

The computer code AX\_LOAD was developed to analyze constrained axial expansion of a fuel string in a CANDU reactor under large break loss of coolant accident (LOCA) conditions. For certain large break LOCAs, the fuel experiences rapid heat up and the differential axial thermal expansion can exceed the available axial gap in the channel. Constrained expansion of the fuel string will then result and further expansion is mainly accommodated by deformation of the fuel string.

The axial loads generated during constrained expansion and the consequential axial deformations are assessed by the AX\_LOAD code. The compliant components modelled include the fuel elements, latch bundle, pressure tube, and bundle junctions. The heat up of the bundle junctions during constrained expansion, as a result of contact between the end fuel pellet and element endcap, is considered. Effects of initial fuel conditions and external forces such as flow, pressure and friction are also modelled.

### 1. INTRODUCTION

During normal operating conditions in CANDU nuclear reactors, there is an axial gap between the inlet bundle and the inlet shield plug. This gap is intended to accommodate any differential thermal expansion of the fuel string relative to the pressure tube during normal operation and also during upset situations that could lead to elevated fuel temperatures. For reactors that fuel against the flow (*e.g.*, Darlington, Bruce A/B), the shifting of the fuel string in this gap in a large break LOCA causes a reactivity insertion and consequently increases the severity of the overpower transient. The effect of fuel string relocation can be reduced by limiting the channel axial gap through a gap management system. However, a small axial gap may not provide sufficient clearance for thermal expansion during the accident resulting in constrained expansion of the fuel string. Constrained expansion will occur if the differential axial thermal expansion of the fuel string relative to the pressure tube exceeds the available gap. This constrained expansion exerts axial loads on the restraining components of the fuel channel (*i.e.*, inlet-end shield plug lugs, rolled-joints, outlet-end latch) and on the fuel string itself.

The AX\_LOAD code (Reference 1) was developed to predict the magnitude of the axial loads generated during constrained expansion to assure channel integrity. In addition to calculating the axial load, AX\_LOAD also predicts the temperature of the bundle junctions in contact with the end fuel pellet. The code calculates the axial load transients and bundle junction temperatures resulting from thermal expansion of the fuel string in a channel for a user specified axial gap and temperature transients which are obtained from a fuel behaviour code simulation of the accident.

## 2. FUEL AND CHANNEL MODEL

In the AX\_LOAD model, the fuel string and channel system is treated as a series of interconnected deformable elements connected in a loop as shown in Figure 1. The fuel string and pressure tube are discretized axially to represent each bundle location. The fuel elements in a bundle are treated as concentric rings that can expand and deform independently. This model geometry is similar to that implemented in the fuel behaviour code FACTAR (Reference 2) which provides the accident temperature transients as inputs. Thermal expansion of each fuel ring is calculated assuming perfect axial and circumferential alignment of the bundles. Each fuel ring is modelled to expand independently, ignoring the restraining effect of the endplates. As the fuel heats up in the event of an accident, it can expand freely to consume the available channel axial gap. No axial load is developed in this stage since sliding friction between fuel and pressure tube (PT) is neglected. Once the gap has been fully consumed, constrained expansion takes place resulting in an axial load being exerted on the channel restraining components and the fuel string itself. The amount of differential expansion in excess of the available gap ( $\Delta L_{ex}$ ) from the expansion of the fuel string ( $\Delta L_F$ ) and PT ( $\Delta L_{PT}$ ) must be accommodated by deformations ( $\delta$ ), satisfying the following relation

$$\begin{aligned} \Delta L_{ex} &= \delta \\ \Delta L_F - \Delta L_{PT} - \text{gap} &= \delta_F + \delta_{PT} + \delta_{LB} + \delta_{BJ} \end{aligned} \quad (1)$$

Four compliant components are considered: fuel element (F), pressure tube (PT), latch bundle (LB), and bundle junction (BJ). The deformations of the fuel element, latch bundle and bundle junctions are defined to be positive in compression while the pressure tube deformation is positive in tension. The channel end restraint components (*i.e.*, end-fittings, shield plugs, liner tubes, rolled joints) are treated as rigid in this model in order to maximize the load predicted. The relative importance of these deformation mechanisms depends on the input transient conditions corresponding to the postulated accident scenario studied.

Because each fuel ring is modelled to expand independently, Equation 1 has to be satisfied for all the fuel rings. Expanding the quantities in Equation 1 to be the axial sum in the channel, the governing equation relating expansion and deformation for each fuel ring is

$$\Delta L_{ex} = \sum_{i=1}^n (\Delta L_{F_i} - \Delta L_{PT_i}) - \text{gap} = \sum_{i=1}^n (\delta_{PT_i} + \delta_{BJ_i}) + \sum_{i=2}^n (\delta_{F_i}) + \delta_{LB} \quad (2)$$

where  $i$  is the bundle index and  $n$  is the number of bundles. Use of the axial sum of the expansions and deformations assumes axial and circumferential alignment of bundles in the fuel channel. The fuel element compression is summed for only  $n-1$  bundles since the latch bundle is treated separately. Models used in the calculation of the expansions and deformations are described in the following sections.

The objective of the AX\_LOAD code is to determine the axial load generated in the fuel string compression process. For each fuel ring, AX\_LOAD solves by iteration for a ring load which provides sufficient deformations to satisfy Equation 2. The total axial load on the channel is then the sum of the individual ring loads. Actually the ring loads are not completely uncoupled due to the presence of the pressure tube and latch bundle deformation terms in Equation 2. These deformations depend on the total axial load (*i.e.*, sum of all ring loads). To uncouple Equation 2 for all the rings, a conservative simplification is made in AX\_LOAD to credit the pressure tube and latch bundle deformation resulting from only the largest ring load ignoring the contribution from the other ring loads.

### 3. EXPANSION MODEL

Thermal effect is the dominant factor influencing the expansion of the fuel elements and pressure tube. Effects of external forces are also considered for completeness. At each time interval in the analyzed accident transient, AX\_LOAD calculates the free expansion of the fuel elements and pressure tube relative to normal operating conditions (NOC) on which the channel axial gap is based. These expansions are completely governed by the inputs transients (*eg.*, temperature and pressure).

#### 3.1 Fuel Expansion

AX\_LOAD models four factors affecting the fuel string expansion: thermal expansion of UO<sub>2</sub>, residual axial clearance inside the fuel element, external forces, and thermal expansion of bundle junctions. Thermal expansion properties of UO<sub>2</sub> from MATPRO 11 (Reference 3) is used in evaluating the thermal expansion of the fuel elements from the start of accident. At normal operating conditions, the fuel pellet temperature radial distribution is approximately parabolic. During the accident, the outer annuli of the pellet experience the largest temperature rise and hence the largest thermal expansion. The fuel thermal expansion is modelled to be governed by the pellet shoulder temperature rise assuming slippage between the UO<sub>2</sub> and the sheath. Use of the fuel shoulder temperature gives a conservative estimate of the fuel expansion as demonstrated in Figure 2 which compares the thermal expansion using temperature rise at various radial locations of the fuel pellet.

The fuel element is fabricated with an axial clearance to accommodate some thermal expansion of the UO<sub>2</sub>. In modelling the residual axial clearance inside the fuel element, the UO<sub>2</sub> expansion is assumed to initially consume the predicted residual clearance at NOC before it causes any fuel string elongation, consistent with the fuel/sheath slippage assumption. Prior to the residual clearance being filled, the change in fuel element is controlled only by the thermal expansion of the sheath. The amount of residual clearance under normal operating conditions (NOC) is the difference between the sheath length and the longest fuel annulus in the ELOCA simulations which treat the fuel pellet as 100 concentric annuli.

Under NOC conditions, the fuel string is subjected to flow dependent external forces such as coolant drag (skin friction and pressure drop). During a LOCA transient, the flow is reduced substantially and the reduction of the coolant drag can result in elongation of the fuel string relative to its NOC length. This effect is considered in the determination of the fuel string expansion. The external compressive load at NOC is an input to the code. Immediately following the break, the mechanical elastic strain under the external load is added to the fuel string length. This is equivalent to assuming the external force is completely removed after time 0 and the fuel string returns to its unstressed length. The contribution to fuel string expansion from thermal expansion of the bundle junctions is also included in the model but its effect is small since the junctions make up only a small fraction of the total fuel string length.

#### 3.2 PT Expansion

Thermal expansion of the PT is much smaller than that of the UO<sub>2</sub> column because of the smaller thermal expansion coefficient of Zircaloy and the smaller temperature rise experience by the PT during the first few seconds of a large LOCA. New experimental data of the axial thermal expansion property of Zr-2.5 wt% Nb pressure tube up to 800°C is implemented. The curve fit equations of the experimental data are:

$$\begin{aligned} \text{first heating: } dL/L &= 10^{-6} \times [ -179.95 + 7.4804(T-24) - 0.01062(T-24)^2 + 1.3 \times 10^{-5}(T-24)^3 ] \\ \text{subsequent: } dL/L &= 10^{-6} \times [ -1261.5 + 8.060538(T-24) - 0.011902(T-24)^2 + 1.5 \times 10^{-5}(T-24)^3 ] \end{aligned}$$

where T is temperature in °C. The expansion in subsequent heating exhibits a larger expansion coefficient because the material has transformed to beta phase material after being heated to 800°C.

In addition to thermal expansion, the effect of external forces such as channel depressurization, coolant drag, feeder loads, and friction between PT and channel end support bearings are also included in the PT expansion model. Of the four external forces, depressurization and friction are found to be the more significant. From experiments, the channel is found to contract axially when pressure is reduced at a rate of approximately 0.16 mm/MPa. When friction is considered, the total axial force on the PT including the effective thermal expansion force of the PT and fuel string expansion force must exceed the friction force between the PT and its end supports before any PT expansion is credited. The friction force, which is an input, is assumed to be constant during displacement of the PT since displacement and velocity are very small. When the friction force is overcome, the amount of PT expansion credited is that from a net resultant force which is the total axial force reduced by the friction.

#### **4. DEFORMATION MODEL**

Four compliant components are modelled to deform in accommodating the excess expansion of the fuel string beyond the available gap: fuel element, latch bundle, pressure tube, and bundle junctions. All other channel components are assumed infinitely rigid to maximize the axial load predicted. The residual axial clearances predicted to exist in the end bundle elements during compression are not considered in the deformation model which assumes the UO<sub>2</sub> column is always supporting the element. The relative significance of the modelled compliant components in accommodating the excess expansion is dependent on the accident transient analyzed.

##### **4.1 Element Deformation**

The fuel elements are modelled to undergo elastic compression as integral elastic beams under an axial load. Local deformation at the pellet interface ridges are not considered. An upper bound of 60 GPa is used as elastic modulus of the fuel element (Reference 4) to give a conservative high estimate for the predicted axial load. In calculating the stress on a fuel element, the axial ring load is assumed shared equally amongst the number of elements in the fuel ring. The cross sectional area of the fuel pellet is held constant in the stress calculation since the expected change is small. Plastic creep of UO<sub>2</sub> is also modelled since it can be an significant deformation mechanism under high temperature and stress conditions.

At high temperatures, there are many factors which would affect the strength of the fuel (Reference 5) making the fuel elements more compliant. With 97% of the fuel string length made up by the UO<sub>2</sub> fuel column, additional compliance of the fuel at high temperatures would greatly alleviate the axial load.

##### **4.2 Latch Bundle Deformation**

Because of its unique support geometry, the latch bundle can behave differently in compression. The load / displacement curve of a bundle compression experiment against a latch at room temperature (Reference 6) is implemented in the code. Applying these room temperature results at the higher temperature encountered in a LOCA should be conservative since the mechanical properties of the materials would be over-estimated.

##### **4.3 PT Deformation**

The pressure tube deformation under axial load is modelled as elastic tension. The modulus of the

Zr-2.5wt% Nb is temperature dependent and therefore each PT axial segment deforms a different amount under the same axial load. Cross sectional area of the PT is kept constant in the stress calculation since its deformation is relatively small. In evaluating the displacement of the PT as a result of the axial load, the friction force between the PT and channel end supports are considered to ensure that the total axial load on the PT exceeds the friction force before any PT elongation is credited to alleviate the constrained expansion.

#### 4.4 Bundle Junction Deformation

Since the fuel element compliance at elevated temperatures is not modelled, bundle junction creep deformation is a significant mechanism in accommodating for the expanding fuel. A typical bundle junction end is illustrated in Figure 3. In order to analyze the deformation in detail, each bundle junction end is discretized into four components of tractable geometry: endplate, spigot, endcap, and projection. The deformation of a junction at a bundle location is twice the sum of the deformation of all the components to account for the two ends in a junction:

$$\delta_{BJ_i} = 2 \{ \delta_{\text{endplate}_i} + \delta_{\text{spigot}_i} + \delta_{\text{endcap}_i} + \delta_{\text{projection}_i} \} \quad (3)$$

Deformation of the bundle junction components is modelled as material creep. The incremental junction component (projection, endcap, spigot, and endplate) deformation in a time interval is determined from the component creep rate and duration of the time interval.

$$\delta_{BJ_i}(t+\Delta t) = \delta_{BJ_i}(t) + \Delta\delta_{BJ_i}; \quad \Delta\delta_{BJ_i} = \dot{\epsilon}_{BJ_i}(\sigma, T) \Delta t L_{BJ_i} \quad (4)$$

where BJC = bundle junction component (spigot, endcap, projection, endplate)  
 $\dot{\epsilon}$  = creep rate  
 $\Delta t$  = time interval  
 $\sigma$  = applied stress  
 $T$  = temperature

The creep rate is primarily a function of applied stress and temperature. Although all bundle junction components of the same fuel ring in the channel are subject to the same ring load, they can have different applied stresses depending on the load bearing area. Stiffening of the junction component during compression as a result of cross sectional area increase is modelled. Conservation of volume is used to relate the change in cross sectional area to the axial deformation. The temperature of the bundle junction components are evaluated in a junction thermal model in AX\_LOAD.

Once the temperature and axial stress of a bundle junction component is known, its creep rate is evaluated using the microstructural creep law COZY (Creep Of Zircaloy) (Reference 7). Most of the predicted junction deformations occur at the projections because of the high temperature from the proximity to the fuel and high stress from the smaller cross sectional area.

## 5. BUNDLE JUNCTION THERMAL MODEL

A thermal model of the bundle junction is implemented in AX\_LOAD since the junction temperatures are not available as inputs. The bundle junction is discretized into four lumped parameter volumes corresponding to the four junction components in the deformation model. In essence, the model considers the axial heat flow from the end pellets to the junction using the temperatures of the fuel, sheath, and coolant calculated by the FACTAR code as input boundary conditions. The conduction equations are

solved using a finite difference approach to provide the transient bulk temperatures of the endplate, spigot, endcap and projection.

In order to model both the steep temperature gradients which can form at the fuel ends in response to heat removal to the endcap and the increased temperature due to end flux peaking, the fuel volume in contact with the endcap is discretized into fine node volumes. The number of fuel nodes axially and radially and their spacing are defined in the inputs to the code. Figure 4 shows the nodalization scheme of the thermal model.

### 5.1 Boundary Conditions

The input temperature histories of the sheath and coolant define the temperature at these reference nodes. The fuel nodes axially farthest from the endcap are also treated as reference nodes with defined temperatures. However, the input fuel temperature histories represent fuel temperatures at the fuel element mid-plane. To save computational time, the thermal model usually considers a smaller axial length of fuel. To adjust these input temperatures to be representative of the fuel element ends in the thermal model, the temperature difference from the input fuel centreline to fuel surface at the mid-plane was increased by the flux peaking factor, which is a function of the distance from the endcap (Reference 8), to represent the fuel temperatures at the reference fuel nodes.

### 5.2 Thermal Solution

The remaining node temperatures are derived from the heating rate which is evaluated in finite difference form as:

$$\frac{dT_i}{dt} = \frac{\sum_j (T_j - T_i) h_{ij} A_{ij} + (HV)_i}{(C_p V)_i} \quad (5)$$

where  $T_i$  is the current node temperature,  
 $T_j$  is an adjacent node temperature,  
 $h_{ij}$  is the thermal conductance from node i to node j,  
 $A_{ij}$  is the heat transfer area between node i and node j,  
 $C_p$  is the specific heat  
 $H$  is the volumetric heat generation rate at the current node, and  
 $V$  is the volume of the current node.

The thermal conductance  $h_{ij}$  is the overall thermal conductance from node i to node j, accounting for thermal conductivity of the material(s), and heat transfer coefficients of the interfaces, if applicable. Depending on the nodes involved, the thermal conductance  $h_{ij}$  can be thermal conductivity of UO<sub>2</sub> or Zircaloy, or an interfacial heat transfer coefficient such as junction to coolant, fuel to sheath, or fuel to junction. Transients of the fuel to sheath and sheath to coolant heat transfer (which is used for junction to coolant) coefficient are inputs.

The contact conductance between the fuel and the endcap is derived from a mechanistic model accounting for radiation, gas conductance, and solid/solid conductance (Reference 9). During constrained expansion, the fuel and endcap are in tight contact under high interfacial pressure and as a result, the solid/solid part of the contact conductance quickly dominates the overall heat transfer coefficient. With this contact pressure sensitive thermal conductance model, the thermal conductance between fuel and endcap is strongly a function of the axial load. This provides a negative feedback effect on the axial load

since as the load increases, higher endcap temperatures will result due to the larger fuel/endcap heat transfer coefficient and consequently reducing the load required to maintain the creep rate of the endcaps.

## 6. AXIAL LOAD DETERMINATION

At each timestep in the simulation transient, the amount of deformation in Equation 1 is known from the excess expansion governed by input transients. To satisfy Equation 2 which is nonlinear, an iteration scheme is used to arrive at a ring load yielding the amount of accommodation required. For conservatism and execution speed, the temperature used in the calculation of the junction creep rate is the temperature at the beginning of the timestep (*i.e.*, heat up during the timestep is not credited). In this approach the thermal model is called only once outside the load iteration loop after the ring load has converged.

Sample AX\_LOAD outputs for a large LOCA simulation are shown in Figures 5 and 6. The excess expansion is initially accommodated by the elastic deformation of the fuel and PT. At about 2.8 seconds into the transient, the junction stress and temperature are sufficient to activate significant creep deformation to accommodate the expanding fuel string.

## 7. CONCLUSIONS

The AX\_LOAD code has been used in assessing constrained axial expansion in CANDU reactor analyses. Verification and validation of the code are in progress. Preliminary experimental data from single element axial compression experiments indicate a large margin of conservatism in the modelling of the fuel element compressibility.

## 8. REFERENCES

- 1 J.K. Chan and F.C. Iglesias, *AX\_LOAD 1.0 Program Manual*, Ontario Hydro NTS Report no. N-03553-940029, April 1994.
- 2 H.E. Sills, S.L. Wadsworth, L.J. Watt, and P.J. Reid, *FACTAR Version 1: Fuel and Channel Temperature and Response Part I: Model Description and User Manual*, Ontario Hydro NTS Report No. N-03553-940031, April 1994.
- 3 D.L. Hagerman et al., *MATPRO-11 (revision 2) A Handbook of Material Properties for Use in the Analysis of Light Water Reactor Fuel Rod Behaviour*, NUREG/CR-0497, August 1981.
- 4 J.H.K. Lau et al., *Minimum Gap Requirements Between Fuel String and Shield Plug for Postulated Accidents in Ontario Hydro 900MW Reactors*, submitted to AECB November 1993.
- 5 J.K. Chan, Y. Liu, H.E. Sills, V.J. Langman, *High Temperature Fuel Behaviour, Constrained Axial Expansion and the Potential Effects on Fuel Channel Integrity During Large Break LOCAs*, Ontario Hydro Report No. N-03503.7-955045, April 4, 1995.
- 6 M. Gabbani, *Bundle/Latch Deformation Test: Long Bundle Program*, AECL-CANDU File# 29-37000-200-1027, October, 1993.
- 7 H.E. Sills and R.A. Holt, *NIRVANA: A High-Temperature Creep Model for Zircaloy Fuel Sheathing*, AECL-6412, 1979.
- 8 P.M. French, *Measurements of Bundle End Flux Peaking Effects in 37-element CANDU PHW Fuel*, AECL-5968, (1977).
- 9 H.E. Sills, *ELOCA Fuel Element Behaviour During High-temperature Transients*, AECL-6357, March 1979.

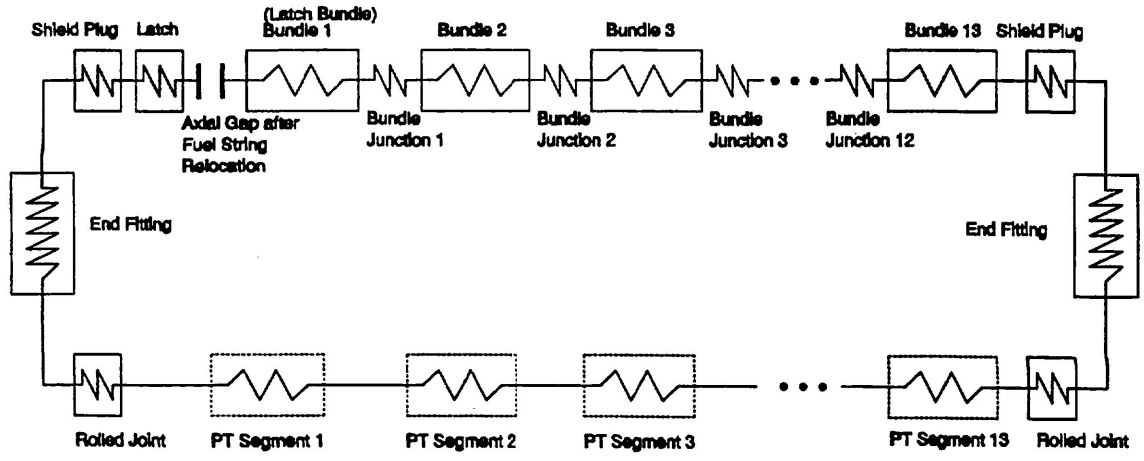


Figure 1: Schematic of Fuel String and Channel Model in AX\_LOAD

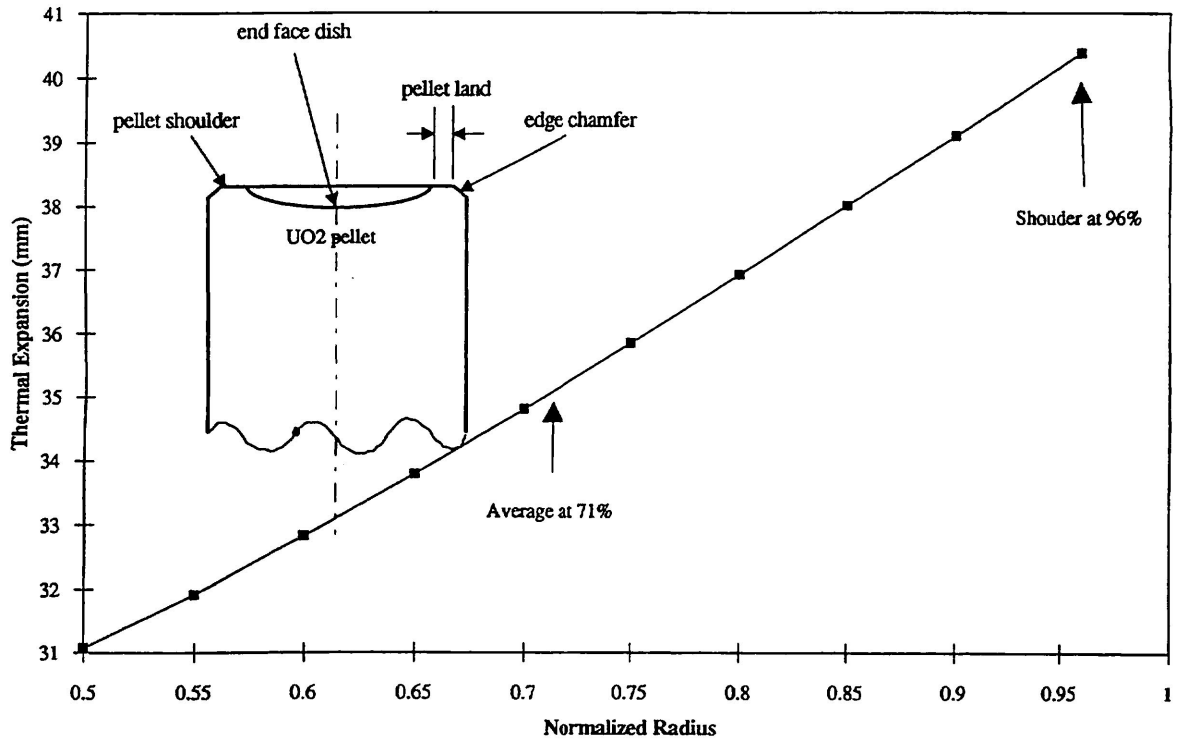


Figure 2: Fuel String Thermal Expansion Using Temperature Rise at Various Radial Locations

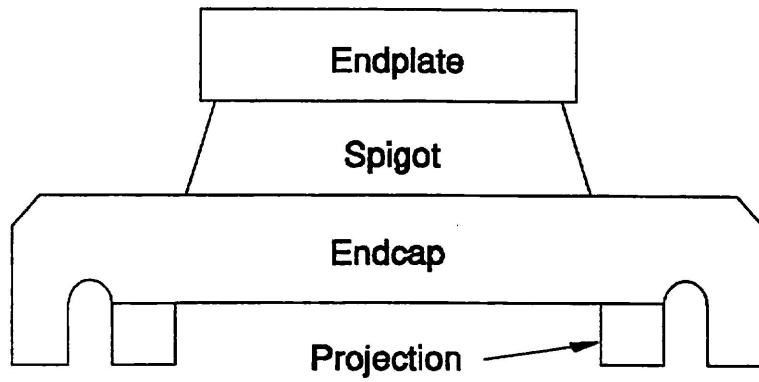


Figure 3: Schematic of Bundle Junction Model with Four Components

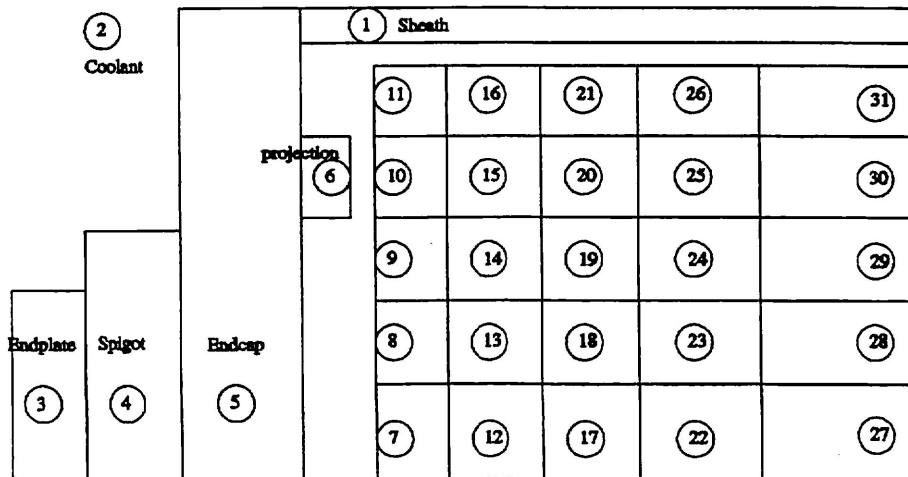


Figure 4: Nodalization of Fuel and Junction Components in Thermal Model

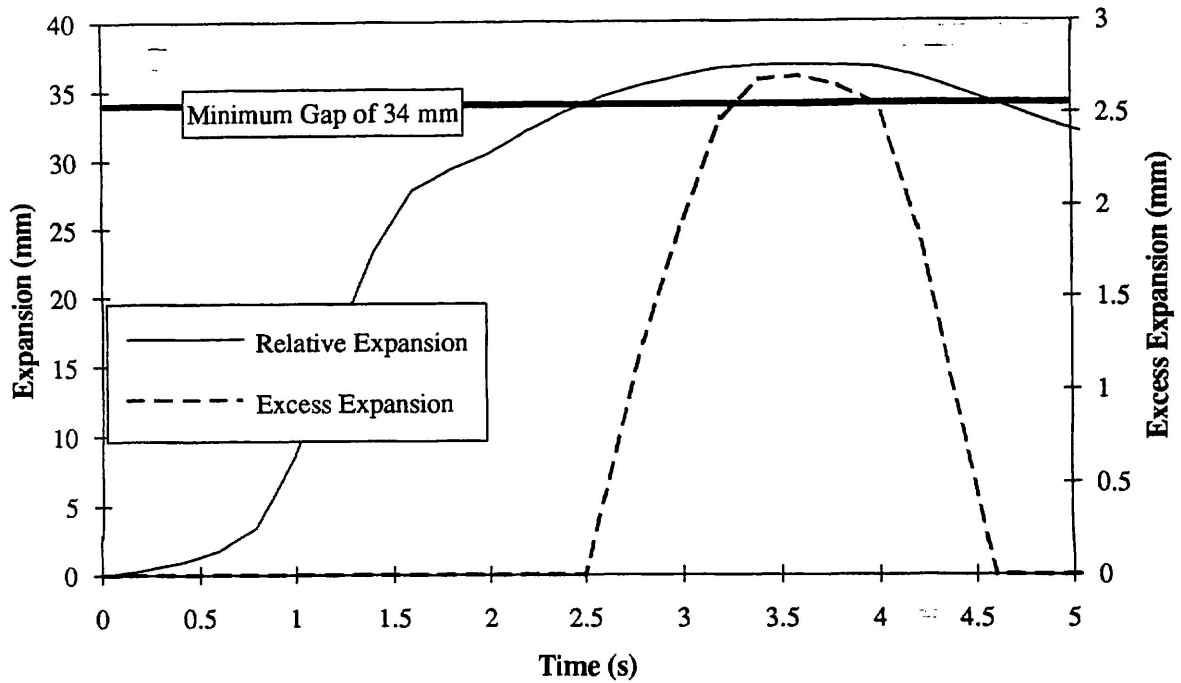


Figure 5: Sample Output Showing Relative Expansion Exceeding Minimum Axial Gap

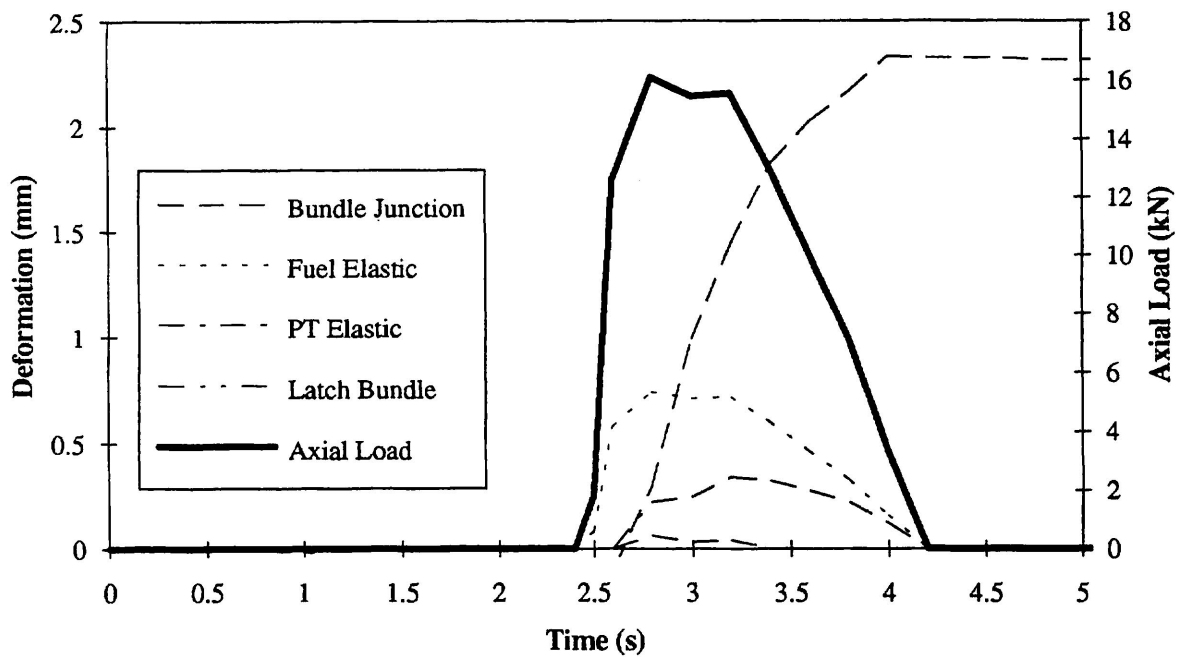


Figure 6: Sample Output of AX\_LOAD Predicted Axial Load and Deformations